ACSNANO
www.acsnano.org
ARTICLE

Interactions between Membranes and "Metaphilic" Polypeptide Architectures with Diverse Side-Chain Populations

Michelle W. Lee,[†] Ming Han,[‡] Guilherme Volpe Bossa,[∥] Carly Snell,[∥] Ziyuan Song,[§] Haoyu Tang,[§,□] Lichen Yin,[§,▲] Jianjun Cheng,[§] Sylvio May,[∥] Erik Luijten,[⊥,#,▽] and Gerard C. L. Wong*[,†,¶,⊗]

[†]Department of Bioengineering, [¶]Department of Chemistry & Biochemistry, [⊗]California NanoSystems Institute, University of California, Los Angeles, Los Angeles, California 90095, United States

[‡]Applied Physics Graduate Program, [⊥]Department of Materials Science and Engineering, [#]Department of Engineering Sciences and Applied Mathematics, [▽]Department of Physics and Astronomy, Northwestern University, Evanston, Illinois 60208, United States

[∥]Department of Physics, North Dakota State University, Fargo, North Dakota 58108, United States

[§]Department of Materials Science and Engineering, University of Illinois at Urbana−Champaign, Urbana, Illinois 61801, United States

Supporting Information

ABSTRACT: **At physiological conditions, most proteins or peptides can fold into relatively stable structures that present on their molecular surfaces specific chemical patterns partially smeared out by thermal fluctuations. These nanoscopically defined patterns of charge, hydrogen bonding, and/or hydrophobicity, along with their elasticity and shape stability (folded proteins have Young's moduli of ~1 × 10^8 Pa), largely determine and limit the interactions of these molecules, such as molecular recognition and allosteric regulation. In this work, we show that the membrane-permeating activity of antimicrobial peptides (AMPs) and cell-penetrating peptides (CPPs) can be significantly enhanced using prototypical peptides with "molten" surfaces: metaphilic peptides with quasi-liquid surfaces and adaptable shapes. These metaphilic peptides have a bottlebrush-like architecture consisting of a rigid helical core decorated with mobile side chains that are terminated by cationic or hydrophobic groups. Computer simulations show that these flexible side chains can undergo significant rearrangement in response to different environments, giving rise to adaptable surface chemistry of the peptide. This quality makes it possible to control their hydrophobicity over a broad range while maintaining water solubility, unlike many AMPs and CPPs. Thus, we are able to show how the activity of these peptides is amplified by hydrophobicity and cationic charge, and rationalize these results using a quantitative mean-field theory. Computer simulations show that the shape-changing properties of the peptides and the resultant adaptive presentation of chemistry play a key enabling role in their interactions with membranes.**

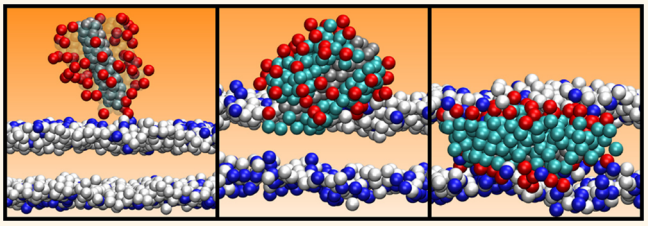

KEYWORDS: *antimicrobial peptides, cell-penetrating peptides, amphiphilic, membranes, peptide−membrane interactions*

The functions of proteins or peptides, such as molecular recognition, enzymatic reactions, and allosteric regulation, are determined by their structures and their internal motions: Proteins or peptides can fold into structures that present specific chemical patterns on their molecular surfaces. These nanoscopically defined patterns of charge, hydrogen bonding, and/or hydrophobicity, which strongly influence peptide or protein interactions, are known to be partly smeared out by thermal fluctuations. For protein configurations structurally cognate to the native folded state, the protein energy surface, which controls protein dynamics, can have multiple minima, and proteins exhibit harmonic motions within these minima as well as crossing of potential barriers between them. In general, however, molecular thermal motions are not large compared to the dimensions of the molecule. Moreover, single-molecule experiments show that folded proteins typically have Young's moduli of ~1 × 10^8 Pa,[1−3] which give the protein a solid-like rigidity. There is a rich literature showing that in the low-temperature limit, proteins can undergo a dynamic transition to a glass-like solid state with small fluctuations.[4,5] Taken together, the surface structure, shape, and elasticity of a protein determine the resultant presentation of surface chemistry, and thereby enable or limit

Received: November 28, 2016
Accepted: February 17, 2017
Published: February 17, 2017

DOI: 10.1021/acsnano.6b07981
ACS Nano 2017, 11, 2858−2871

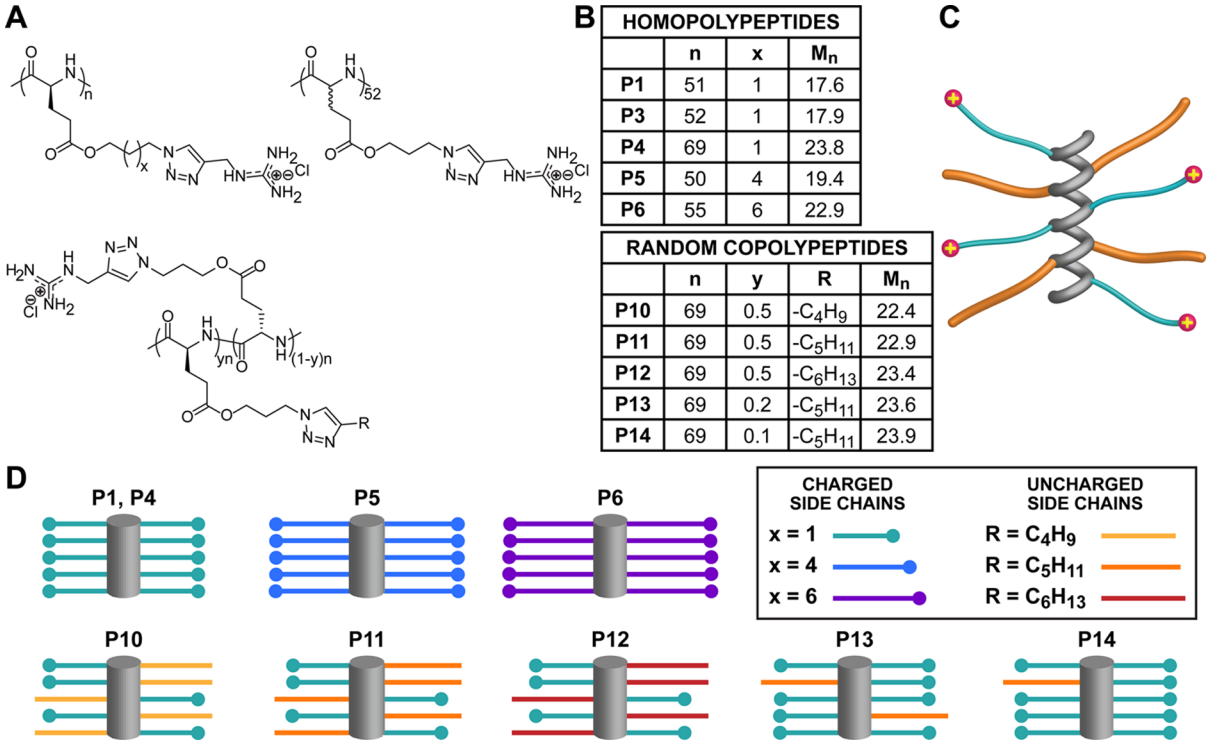

Figure 1. Design of metaphilic helical peptides. (A) Metaphilic helical peptides are poly(arginine) analogues characterized by long hydrophobic side chains (13−18 σ-bonds in length) that have either a terminal guanidinium group or alkyl chain. Charged monomers having guanidinium groups were used to synthesize homopolypeptides (top left). A mixture of charged monomers and uncharged monomers, which feature terminal alkyl chains, were used to synthesize random copolypeptides (bottom). All prepared peptides adopt an α-helical conformation except for P3 (top right), which was synthesized as a random coil from racemic monomers. (B) The structural peptide design parameters include the following: n (degree of polymerization), x (number of methylene groups), y (molar fraction of uncharged monomers), R (terminal alkyl chain), M_n (number-average molecular weight in kDa). (C) Metaphilic peptides featuring long side chains with terminal cationic and alkyl groups favor a stable α-helical conformation in aqueous solution. (D) Simplified cartoon depictions comparing the fractions of charged and uncharged side chains among the various metaphilic peptides.

its interactions. It would be interesting to start with the functional requirements for a given protein or peptide class, and explore the opposite limit, where patches of surface chemistry can be mobile.

Both antimicrobial peptides (AMPs) and cell-penetrating peptides (CPPs) are short (generally <50 amino acids) peptides that exert their functions by interacting with and permeating membranes. As part of the innate host defense, AMPs collectively exhibit broad spectrum antimicrobial activity,[6−8] typically through the disruption and permeabilization of bacterial membranes.[7−10] Although AMPs are abundant and diverse in sequence and structure, they share some common features. Most AMPs are cationic and characterized by facially amphiphilic patterns of hydrophobicity and charge.[6−12] CPPs are capable of efficiently translocating across cell membranes and can mediate the uptake of conjugated cargos.[13−15] CPPs are generally cationic, but can also be amphiphilic, with the arginine-rich CPPs comprising the most widely studied group.[13,15−19] Many CPP sequences are derived from natural proteins and peptides; however, research groups have also developed synthetic CPPs.[13,18] While cationic charge and amphiphilicity are characteristics often found in both AMPs and CPPs, it has been noted that these properties can be found in many other membrane-remodeling peptides,[20] including viral budding peptides[21] and viral fusion peptides.[22] While the vast majority of AMPs and CPPs are composed of linear amino acid sequences, a number of research groups have recently explored unconventional nanoscopic architectures in the design of polymer-based antimicrobial and cell-penetrating agents that are also characterized by cationic charge and hydrophobicity, including circular peptides, and especially an extensive taxonomy of side-chain-rich comb, brush, or dendrimer architectures.[23−28] In this work, we systematically investigate a prototypical class of peptides with side-chain-rich architectures. These peptides consist of a rigid helical core decorated with mobile and flexible side chains that are terminated by cationic and hydrophobic groups, an arrangement that allows cationic and hydrophobic end groups to undergo large displacements, reminiscent of the Lindemann criterion for melting.[29−31] Therefore, these molecules have unusually chemically adaptable and quasi-liquid[32] surfaces. Although one might expect that the loss of well-defined spatial relations between cationic and hydrophobic patches on a highly evolved peptide or protein leads to a degradation of activity, we surprisingly find the opposite. We show that the membrane-permeating activity of AMPs and CPPs, both commonly characterized by anchored cationic and hydrophobic groups, can be significantly enhanced by the highly adaptable side-chain-rich architecture: Like organisms that adapt to different colored environments *via* metachrosis, these molecular architectures adapt to different solvent environments (water, amphiphilic interface, hydrophobic membrane core) by being "metaphilic" rather than statically amphiphilic. In a sense, these metaphilic peptides are a molecular analogue of recently engineered omniphilic/omniphobic surfaces.[35−37] Computer simulations indicate that the quasi-liquid surface of the peptide

DOI: 10.1021/acsnano.6b07981
ACS Nano 2017, 11, 2858−2871

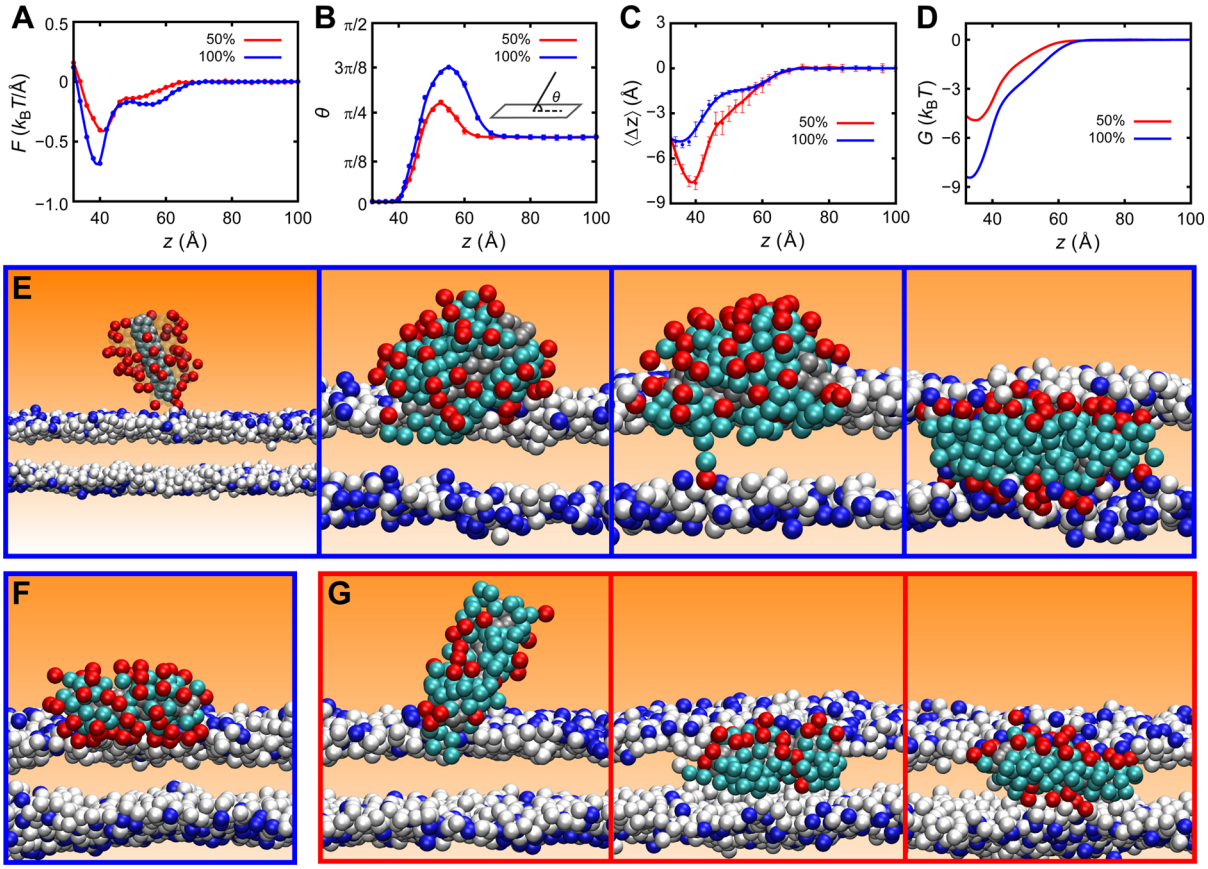

Figure 2. Landing and insertion processes of metaphilic peptides near a membrane. (A) Time-averaged force F exerted on the peptide upon landing. The force is evaluated as a function of the distance z between the center of mass of the peptide backbone and the headgroups of the outer membrane leaflet. Two different cases are compared, in which 50% (red) and 100% (blue) of side chains are terminated by charged end groups. (B) Time-averaged tilt angle θ of the peptide backbone with respect to the membrane plane, as a function of peptide distance to the membrane. Note that tilt angle θ is zero when the peptide is parallel to the membrane and positive otherwise. (C) Averaged deviation $\langle \Delta z \rangle$ of the charged groups from the center of mass of the peptide backbone. (D) Free-energy profile $G(z)$, obtained through integration of the force profile $F(z)$ shown in panel (A). (E) Sequence of simulation images demonstrating landing, initial anchoring (insertion of a side chain into the membrane), initial tunneling (a charged group of a side chain reaching the surface of the inner membrane leaflet), and full insertion in a membrane-spanning state, for a peptide with 4-bead long side chains, of which 100% have charged end groups. Lipid tails and surrounding ions are not shown here. The hydrophobic components of the side chains are colored in cyan, the peptide core is depicted in gray. The remaining beads are color coded based on their charges: red for $+1e$, white for uncharged, and blue for $-1e$. (F) Final state of a peptide with 2-bead long side chains, of which 100% are charged. (G) Sequential images showing initial anchoring, initial tunneling, and full insertion (membrane-spanning) of a peptide with 2-bead long side chains, of which 50% are charged.

allows it to adapt to environmental change by rearranging the flexible side chains, a capability that plays a key role in enabling unusual interactions with membranes. Specifically, these metaphilic peptides are able to induce membrane-destabilizing curvature necessary for permeation, which we determine using X-ray measurements. Furthermore, because these metaphilic molecules can adapt their surface chemistry, we can control their charge and hydrophobicity over a broad range and still maintain water solubility, unlike many AMPs and CPPs.[38−42] This allows us to show how the activity of these metaphilic peptides is amplified with hydrophobicity and cationic charge, and we rationalize these results using a quantitative mean-field theory. One goal of this paper is to develop a general conceptual vocabulary to analyze how molecules of different architectures beyond linear peptides interact with membranes, and how these architectures consequently allow small quantitative changes in structural parameters to lead to qualitative differences in membrane interactions.

RESULTS AND DISCUSSION

Metaphilic Membrane-Active Peptides. We previously developed a series of bottlebrush-like, radially amphiphilic peptides, where hydrophobic side chains that terminate in a cationic group are attached to a rigid core.[43,44] Here we generalize this design and also create peptides with side chains having heterogeneous distributions of cationic and hydrophobic end groups. The surfaces of these brush-like molecules can mimic the chemical surfaces of natural AMPs, but maintain the mobility of cationic and hydrophobic patches so that they can rearrange in response to environmental changes. Specifically, these metaphilic molecules are water-soluble α-helical poly-(arginine)-based polypeptides[45] (Figure 1), which include both homopolymers and random copolymers. The metaphilic peptide monomer features a long hydrophobic side chain with either a terminal guanidinium or alkyl chain that is positioned distally (13−18 σ-bonds away) from the backbone. Increasing cationic residues in a prototypical peptide has been shown to reduce helical stability due to greater electrostatic

DOI: 10.1021/acsnano.6b07981
ACS Nano 2017, 11, 2858−2871

repulsion between side chains[38,39] and increasing hydrophobicity leads to poor water solubility and aggregation.[40−42] In the current architecture, charges are positioned at a significant distance away from the helical backbone to decrease the surface charge density and side-chain repulsion, which promotes their stable α-helical conformation in an aqueous environment.[45] In addition, the charged exterior shell formed by the terminal guanidinium groups around the helical backbone enables the metaphilic peptides to maintain water solubility by shielding the hydrophobic carbon side chains and helical core from solution.

All metaphilic peptides were synthesized through ring-opening polymerization of γ-chloroalkyl-L-glutamate-based *N*-carboxyanhydrides, followed by the conversion of the side-chain chloro groups into azido groups, and the subsequent copper-catalyzed Huisgen click chemistry with propargyl guanidines to attach guanidinium groups at the side-chain terminus.[45] This robust and efficient synthesis enables the control of the side-chain hydrophobicity in two different ways: (1) the variation of methylene spacer lengths between the pendant triazoles and esters through selecting different amino acid precursors (P1, P5, P6); (2) the introduction of additional hydrophobic moieties by coconjugating long chain alkynes together with the propargyl guanidines (P10−P12). The latter also enables the control of charge density by varying the feeding ratios of propargyl guanidines and long chain alkynes (P11, P13, P14).

Metaphilic Peptides Exhibit Adaptable Amphiphilicity upon Interaction with Membranes. We performed generic coarse-grained molecular dynamics simulations to investigate the behavior of these metaphilic peptides as they interact with lipid membranes in an aqueous environment. Specifically, we were interested in the process in which a metaphilic peptide (with either 50% or 100% of its side chains terminated by a cationic end group) approaches a negatively charged membrane surface and subsequently inserts and organizes itself within the phospholipid bilayer.

The adaptation of the peptide configuration and its free-energy variation were quantitatively explored in a steered landing process, as illustrated in Figure 2. At large separation, the peptide barely interacts with the oppositely charged membrane due to electrostatic screening by the ions (Figure 2A), and its backbone effectively behaves as a neutral rod, randomly orienting with an average tilt angle $\theta = \pi/2 - 1$ toward the membrane (Figure 2B). Its affinity to the membrane emerges at separations $z < 68$ Å (defined as the distance between the peptide center and the membrane outer leaflet), around one peptide length. The peptide backbone begins to orient more orthogonally so that some of the charged side chains are able to reach the membrane. Apart from reorienting, the peptide also reorganizes its mobile side chains with their charged end groups extending toward the membrane, giving rise to an asymmetric charge distribution. This asymmetry is reflected in and quantified by the average deviation $\langle \Delta z \rangle$ of the charged end groups from the peptide center (Figure 2C). The tilted peptide touches the membrane and starts to settle at $z = 50$ Å; it fully lies down at $z \sim 40$ Å, reaching its strongest asymmetry. Completion of this "landing" process is marked by the distance at which the forces on the peptide are balanced, near $z_{landing} = 36$ Å. The free-energy changes for the peptides with 50% and 100% charge coverage upon landing are $-4.9k_BT$ and $-8.4k_BT$, respectively (Figure 2D).

Furthermore, we also simulated the free (*i.e.*, nonsteered) landing and insertion process of a peptide with 100% charge coverage, as illustrated in Figure 2E. Initially, the peptide indeed tilts toward the membrane with charged end groups shifted downward, confirming our findings. After landing, the hydrophobic parts of the side chains tend to merge into the hydrophobic interior of the membrane, whereas the charged end groups tend to stay outside. The peptide first "anchors" to the membrane by bending a side chain and partially inserting its hydrophobic part into the membrane. Such a side chain can then further minimize its energy by "tunneling" of its charged end group toward the membrane surface on the inner leaflet. This process provides a strong driving force for the second stage, namely insertion of the peptide to completely span the membrane bilayer.

The insertion process exhibits a strong dependence on side-chain length. From simulations we found that peptides with twice shorter side chains fail to insert (Figure 2F). These side chains are too short to undergo significant adaptation required by the "anchoring" and "tunneling" stages. As a consequence, the hydrophobic parts of the peptide side chains are shielded by the charged end groups and unable to interact with the membrane. This obstacle, however, can be overcome by reducing the charge coverage. As shown in Figure 2G, a peptide with reduced charge coverage of 50% and short side chains can successfully anchor to the interior of the membrane *via* its uncharged side chains. Having uncharged, hydrophobic side chains is sufficient to facilitate insertion and span the membrane. This indicates that membrane insertion is less efficient with shorter cationic side chains. However, it is possible to optimize the efficiency of the peptide by combining high charge coverage to achieve a large landing rate and a finite fraction of uncharged side chains to assist in the hydrophobic insertion process.

Dynamic Adaptability of Metaphilic Peptides Can Enhance Membrane Permeation. Previous studies have suggested that penetration of amphiphilic helical peptides into a bilayer perturbs the hydrophobic interactions of the membrane core, thus leading to membrane destabilization. This process depends on both the hydrophobic content of the peptide and membrane penetration depth. Indeed, the reduction of membrane activity of cationic amphiphilic α-helices has been found to correlate with decreased hydrophobicity.[46,47] Accordingly, the relative sizes of the polar and hydrophobic faces of an amphiphilic helical peptide have been shown to affect the induced membrane curvature.[11,48−53] For metaphilic peptides, there is a wider range of possibilities. Although sometimes AMPs can become amphiphilic and α-helical as they touch down on a membrane,[54] the simulation model here predicts that the metaphilic peptide will undergo a series of structural transitions as it engages the membrane that are not possible for most proteins or peptides: it has uniformly distributed side chains in bulk aqueous solution far from a membrane, but adopts a facially amphiphilic structure near a membrane, with cationic end groups arranged to face toward the membrane surface. Once adsorbed onto the membrane surface, the peptide reorganizes its side-chain components to invert its facial amphiphilicity with cationic end groups associated with the polar lipid headgroups at the surface, while the hydrophobic moieties penetrate further into the membrane core. Depending on the length of the side chains relative to the membrane thickness, terminal groups of the side chains can diffuse through the membrane, so that it is possible for a single metaphilic

DOI: 10.1021/acsnano.6b07981
ACS Nano 2017, 11, 2858−2871

peptide to present guanidinium groups to polar lipid headgroups on *both* leaflets of the membrane, which is not possible for AMPs. These effects lead to two interesting consequences. It is known that details of amphiphilic conformation can play important roles in peptide−membrane interactions necessary for function.[49,57−59] The ability of metaphilic peptides to invert their facial amphiphilicity *via* progressive side-chain migration suggests a direct translocation mechanism with no analogue in natural peptides. Moreover, simultaneous presentation of curvature-generating guanidinium groups to both membrane leaflets may lead to significantly enhanced membrane curvature generation,[60−66] which we explore in the next section.

Metaphilic Peptides Can Induce Negative Gaussian Curvature Necessary for Membrane Permeation. To assess the membrane-permeating mechanism of these peptides, we used high-resolution synchrotron small-angle X-ray scattering (SAXS) to quantitatively characterize the membrane deformations induced by metaphilic peptide variants. Small unilamellar vesicles (SUVs) were prepared from a phospholipid mixture of 1,2-dioleoyl-*sn*-glycero-3-phospho-L-serine (DOPS) and 1,2-dioleoyl-*sn*-glycero-3-phosphoethanolamine (DOPE) at a molar ratio of 20/80. Each metaphilic peptide was incubated with SUVs at a specified peptide-to-lipid (P/L) molar ratio corresponding to an electroneutral P/L charge ratio and the resulting membrane structures were characterized using SAXS.

We found that all α-helical metaphilic peptides (P1, P4−P6, P10−P14) resulted in the restructuring of the lipid vesicles into phases rich in negative Gaussian curvature (NGC) (Figure 3A,B), whereas control samples of SUVs only exhibited a broad characteristic feature consistent with the form factor of unilamellar vesicles. For every helical peptide, we typically observed a coexistence of phases: (1) one set of peaks with integral Q-ratios, which indexed a lamellar (L_α) phase with periodicity in the range of 5.5 to 7.4 nm; (2) a second set of correlation peaks with Q-ratios $\sqrt{1}:\sqrt{3}:\sqrt{4}:\sqrt{7}:\sqrt{9}$, consistent with an inverted hexagonal (H_{II}) phase with a lattice parameter of 6.8 to 8.0 nm; (3) a third set of peaks with characteristic Q-ratios that indexed either a *Pn*3*m* "double-diamond" or an *Im*3*m* "plumber's nightmare" cubic (Q_{II}) lattice, or a coexistence of both. Q-ratios of $\sqrt{2}:\sqrt{3}:\sqrt{4}:\sqrt{6}:\sqrt{8}:\sqrt{9}$ and $\sqrt{2}:\sqrt{4}:\sqrt{6}:\sqrt{8}$ correspond to *Pn*3*m* and *Im*3*m* cubic phases, respectively. In our experiments, cubic phase lattice parameters were found to range from 15.4 to 28.2 nm for *Pn*3*m* and 20.9 to 24.8 nm for *Im*3*m* (Figure 3C,D). For coexisting *Pn*3*m* and *Im*3*m* cubic phases, the ratio of their lattice parameters was close to the Bonnet ratio of 1.279,[67] indicating that the amount of curvature is balanced across the cubic phases, and thus implying that they are close to equilibrium. A bicontinuous cubic phase, such as *Pn*3*m* and *Im*3*m*, consists of two nonintersecting aqueous regions separated by a lipid bilayer that traces out a periodic minimal surface. All points along this minimal surface have NGC, which is also known as saddle-splay curvature due to its shape—the surface bends upward in one direction and bends downward in the orthogonal direction. NGC is topologically required for processes such as pore formation, budding, blebbing, and vesicularization,[21,63,64,68] all of which destabilize and compromise the barrier function of membranes. In fact, for molecules and peptides with functions determined by their membrane-disrupting activity, a strong correlation has been identified between NGC generation and their activity. For example, AMPs generally kill bacteria by inducing membrane permeabilization.[6−9,69] Recent studies have shown the trend of NGC

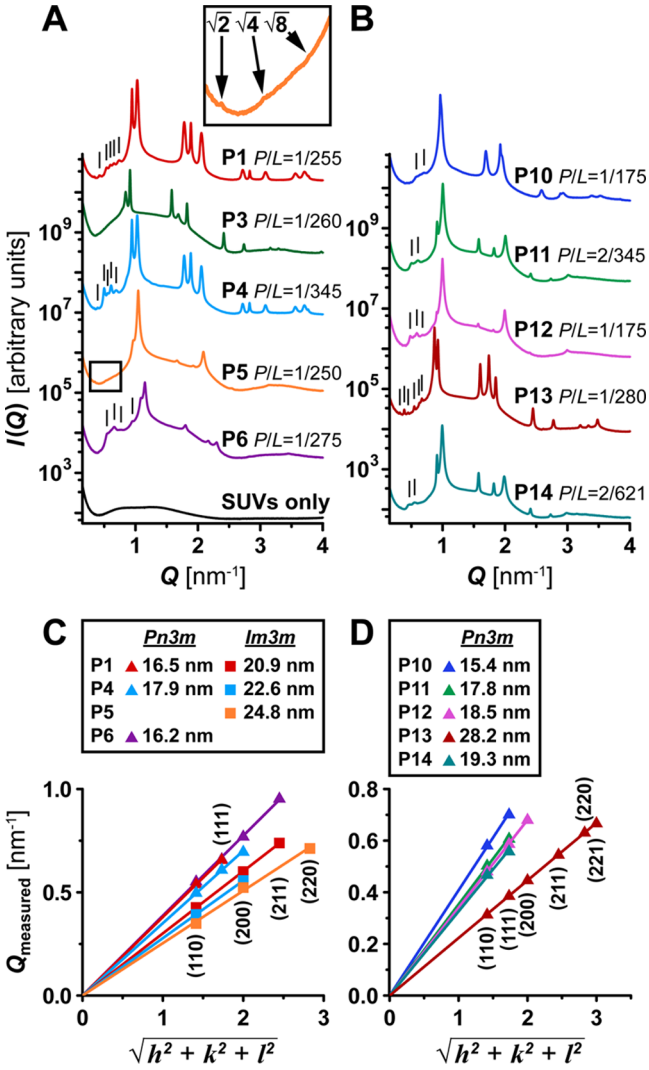

Figure 3. Metaphilic helical peptides generate NGC necessary for membrane permeation. SAXS spectra from DOPS/DOPE = 20/80 membranes incubated with homopolymer (A) and random copolymer (B) peptides at electroneutral P/L molar ratios. Correlation peaks corresponding to identified cubic phases are indicated (black lines). Inset in (A) provides an expanded view of the cubic reflections (boxed region) for P5. (C,D) Indexing of the peptide-induced *Pn*3*m* and *Im*3*m* cubic phases is shown by plotting the measured Q positions, $Q_{measured}$, *versus* the assigned reflections in terms of Miller indices, $\sqrt{(h^2 + k^2 + l^2)}$. The slopes of the linear regressions were used to calculate their lattice parameters, which are listed in the legends.

generation and membrane permeation for a large number of α-helical AMPs,[60,63] AMP mutants,[60,65] and synthetic AMP analogues.[70−72] Similarly, this trend has also been observed for a range of CPPs and transporter sequences.[61,62,64,66] We found that the amounts of NGC generated by the present metaphilic peptides are comparable to those generated by AMPs[60,63] and CPPs.[61,62,64,66] From the simulation data, it is clear that metaphilic peptides can interact with membranes in ways that many peptides cannot. However, the SAXS results above show that metaphilic peptides retain the ability to permeabilize membranes like AMPs and CPPs.

We find that the inducible asymmetric shape of these metaphilic peptides is necessary in facilitating NGC and membrane permeation activity. Nonhelical P3, a random-coil

DOI: 10.1021/acsnano.6b07981
ACS Nano 2017, 11, 2858−2871

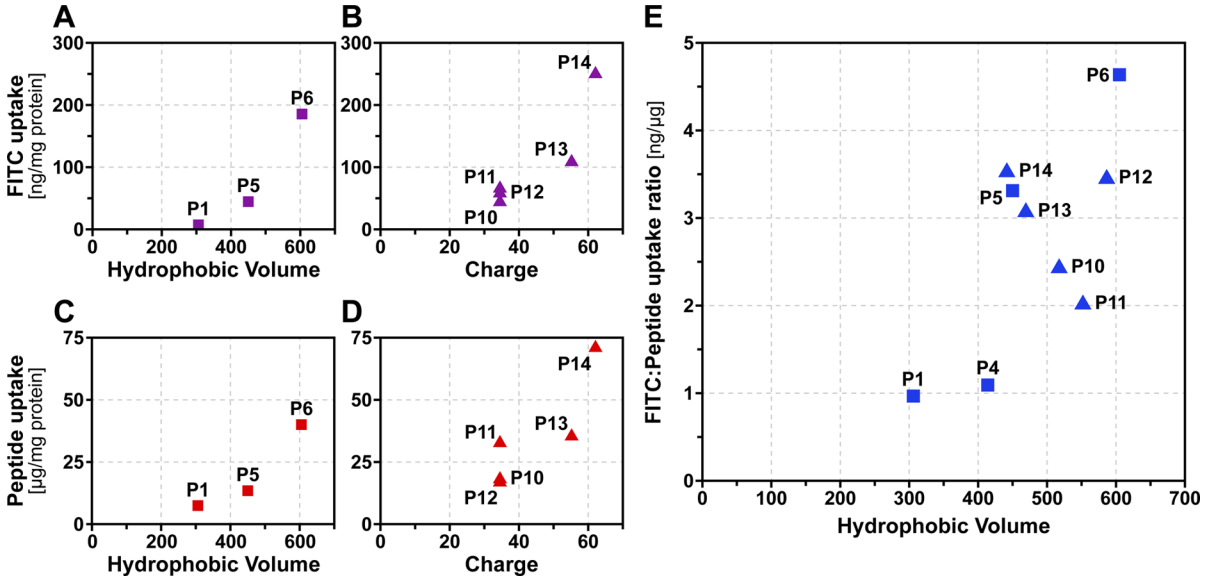

Figure 4. Relations of membrane permeation with hydrophobic volume and cationic charge. Membrane permeation, as measured by FITC and peptide uptake in cells, was found to correlate with the hydrophobic volumes and cationic charges of metaphilic helical peptides. A set of homopolypeptides (P1, P5, P6) with similar degree of polymerization and charge exhibited both FITC (A) and peptide (C) uptake levels that tracked well with their different hydrophobic volumes. Conversely, a set of random copolypeptides (P10−P14) with identical degree of polymerization and comparable hydrophobic volumes showed that increasing cationic charge correlated with increased FITC (B) and peptide (D) uptake. (E) Among all nine metaphilic helical peptides tested, we also observed that the ratio of FITC uptake to peptide uptake generally increased with hydrophobic volume. Greater hydrophobic volumes promote more stable pores with longer lifetimes, which allow more efficient membrane permeation by free molecules of peptide and FITC. In contrast, lower hydrophobic volumes are expected to yield more transient pores with shorter lifetimes, and thus, facilitate rapid translocation of the peptide across a membrane.

peptide synthesized from racemic monomers[45] and cognate to metaphilic peptides considered here, was not able to generate NGC, although it is able to interact with the membrane to induce lamellar and inverted hexagonal phases (Figure 3A). Consistent with this, P3 demonstrated significantly lower membrane permeability.[45] Together, these results suggest that the asymmetric elongated shape stabilized by the rigid helical backbone is important for membrane permeation.

A Critical Comparison of Membrane Activity of Metaphilic Peptides, AMPs, and CPPs. We assessed the membrane permeation of a broad range of metaphilic peptides displaying different side-chain lengths, types, and distributions. Peptide uptake alone and fluorescein isothiocyanate (FITC) uptake, when coincubated with peptide, were measured in HeLa cells in previous experiments.[45] FITC, a membrane-impermeable fluorophore, has been used to evaluate peptide-induced pore formation in cell membranes, as the presence of pores allows molecules to enter cells *via* diffusion.[73,74] The results show that all of the α-helical metaphilic peptides exhibited membrane permeability, which is in agreement with our SAXS measurements showing that they are able to induce the curvature required for such membrane activity. In addition, the membrane permeabilities of the peptides were all found to be higher than those of well-known arginine-rich CPPs such as a domain of the human immunodeficiency virus type 1 tranactivator of transcription protein (HIV-TAT) and nona-arginine (R9).[45]

Among the helical homopolypeptides (P1, P4−P6), P6 had the longest charged side chains and resulted in the highest FITC and peptide uptake levels.[45] We hypothesize that this is due in part to its metaphilic presentation of guanidinium groups to the lipid headgroups of both inner and outer leaflets, which can promote efficient generation of curvature at both membrane locations.[60−66] The longer hydrophobic side chains also allow deeper membrane penetration and membrane spanning, which can further facilitate membrane curvature and destabilization[48,49,51] (see below). Previous work has similarly suggested that a greater number of arginines results in stronger membrane curvature effects[60−62,75] and that arginine side chains can penetrate into the membrane interior due to attraction to the phosphate groups on the distal leaflet of the bilayer, leading to the formation of transient pores.[75−78] Consistent with this picture, metaphilic peptides with shorter side chains that cannot span the membrane generally have lower uptake activity.

We specifically compared helical metaphilic peptides with similar degrees of polymerization and cationic charge (P1, P5, P6) and found that both their FITC and peptide uptake levels tracked with their hydrophobic volumes (Figure 4A,C). (See Methods for definitions and calculations of hydrophobic volume.) Among metaphilic peptides with similar levels of hydrophobic volume (P10−P14), we observed that membrane permeation activity increased with increasing cationic charge (Figure 4B,D). We further identified a more general relation among all tested helical metaphilic peptides, namely, that increases in the hydrophobic volume resulted in a higher ratio of FITC uptake to peptide uptake (Figure 4E). We hypothesize that these identified trends can be explained by differences in AMP *vs* CPP behavior, and differences in how free dyes and free peptides translocate into cells.

In these experiments, FITC molecules and peptides are not conjugated to one another, so both can diffuse independently in solution when coincubated with cells. In order for FITC molecules to enter cells, the peptides need to form sufficiently stable pores in the membrane to allow free FITC to pass through. AMPs typically permeate membranes by forming

DOI: 10.1021/acsnano.6b07981
ACS Nano 2017, 11, 2858−2871

transmembrane pores,[79,80] and therefore, free molecules of AMPs or FITC are able to gain access to the cell interior through those pores. The membrane-associated peptides that create the pores themselves can also stochastically translocate into the cell as the pores close.[79,81] In general, the lifetimes of membrane pores can vary greatly,[77,79] with transient pores allowing only a few peptides to translocate before closing, and more persistent pores allowing both membrane-associated peptides and free molecules through.[76] AMPs generally contain more hydrophobic residues than CPPs and generate stable membrane pores,[62,79,80] whereas CPPs are less hydrophobic and cross membranes quickly *via* transient pores.[61,62] Therefore, synthetic peptides that have sufficient hydrophobicity can exhibit AMP-like behavior and insert into the membrane to create transmembrane pores that allow transport across membranes. In contrast, synthetic peptides with low hydrophobicity can behave like CPPs, which are able to translocate across membranes *via* transient membrane permeation.[15,62,75,82,83]

We observed that greater peptide hydrophobic volume generally results in increased uptake of both FITC and peptide. Previous work has shown that increasing the hydrophobicity of CPPs enhances their interaction with the membrane, in turn affecting their behavior, which can change from rapid translocation across membranes to inducing slow leakage of dye from vesicles.[61,62,84] This finding suggests that hydrophobicity, which increases affinity for the membrane core and promotes deeper membrane penetration, can aid in stabilizing peptide-induced pore formation and yield longer pore lifetimes.[61,62,77,84] By increasing the time that a membrane pore remains open, small molecules such as FITC, as well as free peptides in solution that are not membrane-associated, can flow through into the cell. However, there is the potential trade-off between stable pore formation and translocation across a bilayer. As hydrophobicity enhances association of the peptide with the membrane interior to create a stable pore, it also impairs internalization of the peptide due to the greater chance of being retained in the membrane core.[18,61,77,84,85] This reciprocity provides a hypothesis as to why we see the ratio of FITC uptake to peptide uptake generally being higher for peptides with greater hydrophobic volume. As previously mentioned, increased peptide hydrophobicity predominately facilitates increased uptake of both FITC and free peptides, yet attenuates the translocation of lipid-associated peptides that compose the pores. Conversely, we expect lower hydrophobicity to inhibit the uptake of free molecules, and instead, promote internalization of membrane-associated peptides. Thus, a compensatory exchange exists between free peptide uptake and lipid-associated peptide uptake, which together constitute the total measured peptide uptake. Understandably, because FITC uptake requires stable pores, the effects of peptide hydrophobicity would be more prominent for FITC uptake in comparison to peptide uptake. As a result, the observed relationship between hydrophobic volume and the ratio of FITC uptake to peptide uptake will reflect that of hydrophobicity and FITC uptake. We also found that both FITC and peptide uptake increased with increasing cationic charge. The initial step for cellular entry of either molecule involves electrostatic interactions between the peptide and the membrane surface.[15,86−88] Therefore, increased positive charge can promote more efficient binding of the peptide to the negative charges on the cell surface, which can subsequently enhance overall membrane permeation and cellular uptake.[15,39,87] Finally, it is important to note that the cationic charge specifically for the metaphilic peptides originates from their guandinium groups. Interestingly, the guanidinium group of arginine has been found to play a key role in CPP membrane permeation,[89,90] and an increased number of arginines increases both the ability to generate NGC and cellular uptake.[16,60−62,75,90,91] All of these findings are in agreement with our observations here.

Metaphilic Peptide Behavioral Trends Consistent with Mean-Field Description. We further characterized the ability of metaphilic peptides to induce NGC by a simple mean-field model. The model is an extension of the opposing-forces model,[92,93] supplemented by a hydrocarbon chain free energy that reflects the packing of the lipid tails in a bilayer geometry.[94,95] Specifically, each lipid is characterized by its cross-sectional area a_i at the polar−apolar interface, its cross-sectional area a_h at the headgroup region (measured at fixed distance l_h away from the polar−apolar interface), and the effective hydrocarbon chain extension b; see Figure 5A. The lipid free-energy model (see Methods for details) features

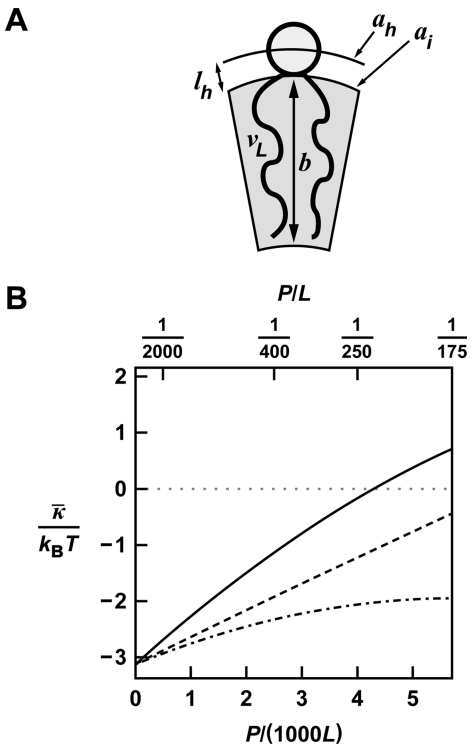

Figure 5. Membrane insertion of a metaphilic peptide results in a less negative Gaussian modulus. (A) We characterize a lipid molecule in terms of the cross-sectional area a_i at the hydrocarbon chain-headgroup interface, the cross-sectional headgroup area a_h (measured at a surface parallel to the hydrocarbon chain-headgroup interface at distance l_h away), and the effective thickness b of the hydrocarbon chain region. The volume v_L occupied by the lipid's two hydrocarbon chains is conserved. The polar headgroup is represented by a light-shaded circle. (B) The Gaussian modulus (measured in units of the thermal energy unit k_BT) as a function of the peptide-to-lipid ratio P/L. The full molecular model (solid line) accounts for both the increase in the hydrophobic volume of the membrane core upon peptide insertion and electrostatic interactions of the anionic lipid headgroups with the cationic terminal groups of the metaphilic peptide side chains. This is contrasted with ignoring either the hydrophobic peptide volume (v_P = 0, dashed line) or electrostatic interactions (dash-dotted line).

DOI: 10.1021/acsnano.6b07981
ACS Nano 2017, 11, 2858−2871

"opposing forces" due to the presence of repulsive interactions between lipid headgroups and a chain-stretching penalty, which are both counterbalanced by a surface tension that acts at the polar−apolar interface.

For any membrane curvature, the conformation of the membrane can be energetically optimized, subject to conservation of the hydrophobic lipid volume v_L. This allows calculation of the Gaussian modulus $\bar{\kappa}$. Note that negative $\bar{\kappa}$ implies a stable bilayer. When $\bar{\kappa}$ becomes positive, the membrane tends to spontaneously adopt saddle-like conformations that are characterized by NGC. We chose model parameters of our molecular free energy that are typical for a lipid bilayer with 20 mol % charged lipids ($\phi = 0.2$), obtaining a Gaussian modulus $\bar{\kappa} = -3.1 k_B T$.

Inserting metaphilic peptides into the lipid bilayer with a peptide-to-lipid ratio P/L will perturb the host lipid bilayer and thus alter $\bar{\kappa}$. Within our mean-field framework, we account for two different types of perturbation. The first originates from insertion of the hydrophobic moieties of the peptide into the hydrocarbon core of the lipid bilayer, and the second relates to the electrostatic interactions of the charged terminal groups of the peptide side chains with the anionic lipid headgroups. Our model describes the former as an effective increase of the hydrophobic lipid volume $v_L \rightarrow v_L + v_P P/L$ where v_P is the hydrophobic volume of the peptide. The latter is quantified based on the Poisson−Boltzmann model, which describes free energies of charged surfaces in an electrolyte solution as a function of their effective surface charge density.

We used model parameters that reflect a typical experimental situation, with $\phi = 0.2$, a hydrophobic peptide volume $v_P = 15$ nm^3, and $z_c = +35$ charges per peptide. Figure 5B shows the Gaussian modulus $\bar{\kappa}$ as a function of P/L from $P/L = 0$ to $P/L = 1/175$. The maximal value $P/L = \phi/z_c = 1/175$ reflects electroneutrality of the membrane. Membrane destabilization is absent when the hydrophobic volume of the peptide is assumed to vanish (dash-dotted line) or when electrostatic interactions are ignored (dashed line). However, when both perturbation modes are accounted for (solid line), the Gaussian modulus adopts a positive sign.

Deep insertion of the peptide into the hydrocarbon core of the membrane tends to not only increase the membrane thickness, but also increase the cross-sectional area per lipid. Yet, a larger cross-sectional lipid area implies weaker mutual headgroup repulsion and an increased surface tension energy at the polar−apolar interface. Hence, we expect the membrane to seek a deformation mode that decreases a_i even if at the same time a_h increases. This is accomplished by a saddle deformation. The electrostatic neutralization of the anionic lipid headgroups by the terminal groups of the metaphilic peptide side chains further lowers the headgroup repulsion strength and, therefore, even more so enhances the tendency of the membrane to minimize its free energy by adopting NGC.

In our mean-field description above, we found that their facially amphiphilic structural organization allows metaphilic peptides to penetrate deeply into the membrane and render the Gaussian modulus less negative. In addition, peptides with cationic charges also shift the Gaussian modulus to less negative values. Both of these changes in the membrane Gaussian modulus are destabilizing and promote NGC generation, which is necessary for membrane permeation. These mean-field trends are in agreement with SAXS measurements and cell uptake results. In fact, these trends are strikingly similar to those observed for AMPs.[60,63,70,71] Here we see that these metaphilic peptides give us a valuable perspective: It is not possible to vary hydrophobicity and charge of many AMPs and CPPs over a large range due to solubility and stability issues.[38−42] However, the adaptable architecture of metaphilic peptides can accommodate greater cationic charge and hydrophobicity. As a result, these are ideal systems for testing how physicochemical properties impact membrane activity, as the above comparison shows. Further details on the molecular model can be found in Methods and Supporting Information.

CONCLUSIONS AND PROSPECTS

Membrane-permeating peptides such as AMPs and CPPs are usually composed of linear sequences of amino acids and have simple architectures. By using a class of peptides with a chemically adaptive metaphilic architecture, which have quasi-liquid surfaces and highly deformable shapes, we showed that it is possible to interact with the membrane in unexpected ways, and significantly enhance the membrane-permeating activity of linear arginine-based peptides. The root causes of this enhancement are explored using a combination of computer simulations, X-ray diffraction, and mean-field theory. Since the metaphilic architecture allows for permeation and translocation mechanisms not available for most peptides, these results here suggest that it may be possible to engineer nanoscopic molecular architectures optimized for applications such as antimicrobial agents for multidrug-resistant bacteria and drug delivery systems.

METHODS

Synthesis of Polypeptides. All peptides (P1, P4−P6, P10−P14) were previously synthesized and characterized elsewhere.[45] The synthesis procedures are outlined in Scheme S1 of the Supporting Information. Typically, L-glutamic acid (1 equiv) was monoesterified using various chloroalkyl alcohols (1.5−2 equiv) under the catalysis of H_2SO_4. The resulting γ-chloroalkyl-L-glutamic acid was purified by recrystallization in deionized water/2-propanol (1:1, v/v) and lyophilized (yield 30−70%). The lyophilized amino acid (1 equiv) was then reacted with phosgene (80% solution in toluene, 1.2−1.5 equiv) in anhydrous tetrahydrofuran (THF) at 50 °C for 2 h to yield γ-chloroalkyl-L-glutamate-based *N*-carboxyanhydrides (NCAs), which were further purified through recrystallization in THF/hexane (1:1, v/v, three times) (yield 60−70%). The dried NCA monomers were transferred into a glovebox and stored at −30 °C.

To obtain the target polypeptides, hexamethyldisilazane was used to initiate the controlled ring-opening polymerization of NCAs in anhydrous dimethylformamide (DMF),[43,96,97] where the degree of polymerization was predetermined by the feeding monomer-to-initiator ratio. After >99% monomer conversion (monitored by Fourier transform infrared spectroscopy), an aliquot of the DMF solution was transferred to a new vial, diluted, and injected into gel permeation chromatography (GPC) for the determination of degree of polymerization and polydispersity (polydispersity <1.26 for all polymers). NaN_3 was then added (10 equiv compared with side-chain chloro groups) and the mixture was stirred at 60 °C for 48 h. The resulting azide-functionalized polypeptide was purified through extraction with chloroform, and subsequent precipitation in hexane/diethyl ether (1:1, v/v) (yield 70−85%). For the final copper-catalyzed click chemistry step, azide-functionalized polypeptide (1 equiv of azido groups) was mixed with propargyl guanidine (1.5 equiv), *N*,*N*,*N*′,*N*′,*N*″-pentamethyldiethylenetriamine (0.10 equiv), and CuBr (0.01 equiv) in DMF in a glovebox. The mixture was stirred at room temperature for 24 h, and the final guanidine-functionalized metaphilic peptide was purified by dialysis against deionized water followed by lyophilization (yield 60−70%). To incorporate additional hydrophobic moieties (P10−P14), long chain alkynes were added together with propargyl guanidine for coconjugation. Azide-functionalized polypep-

DOI: 10.1021/acsnano.6b07981
ACS Nano 2017, 11, 2858−2871

tides were characterized by nuclear magnetic resonance (NMR) and GPC for their chemical structures and molecular weights. The polypeptides post click chemistry side-chain modification were analyzed by NMR to verify the efficiency of side-chain modifications and by circular dichroism to analyze their conformation.[45]

Simulation Procedure. We performed molecular dynamics simulations using the Lammps package to investigate the landing and subsequent insertion process of prototypical metaphilic peptides on and into a membrane.

In our coarse-grained model, all molecules were represented as assemblies of spherical beads (diameter σ = 8.5 Å,[98] the size of a lipid headgroup). Specifically, the membrane was modeled as a bilayer of 4-bead long lipids and spanned an entire cross-section of the system. 20% of the lipids carried a $-1e$ charge on their headgroup. The peptide possessed a helical core of 55 beads (corresponding to 55 amino acids), onto each of which was grafted a 4-bead long, flexible side chain. Either 50% or 100% of the side chains carried a terminal $+1e$ charge. Both the membrane and the peptide were embedded in a 100 mM salt solution mimicking physiological conditions. A relatively large system of size $60 \times 60 \times 60\sigma^3$ was chosen, giving rise to 7200 lipids and over 17 000 ions. Periodic boundary conditions were applied in all three dimensions.

The beads in the peptide core were grouped as a rigid body, whereas those in the side chains or in the lipids were stiffly bonded by a harmonic potential,

$$U_{\text{bond}}(r) = k_{\text{bond}}(r - r_0)^2$$

with equilibrium bond length $r_0 = \sigma$ and strength $k_{\text{bond}} = 300k_BT/\sigma^2$. For lipids, a strong angle potential was introduced between two adjacent bonds to maintain a linear structure,

$$U_{\text{angle}}(\theta) = k_{\text{angle}}(\theta - \theta_0)^2$$

with $\theta_0 = 180°$ and $k_{\text{angle}} = 10k_BT/\text{rad}^2$. All nonbonded beads were subject to excluded-volume effects and Coulomb interactions. The former were implemented *via* a shifted-truncated Lennard-Jones (LJ) potential with strength $\varepsilon = 0.8k_BT$ and cutoff $r_c = 2^{1/6}\sigma$, while the latter was treated *via* Ewald summation with a relative accuracy of 10^{-4}. Moreover, we employed a widely used generic model with implicit solvent to efficiently account for hydrophobicity.[99] Uncharged beads in the hydrophobic side chains and lipid tails experienced an effective attraction,

$$U_{\cos}(r) = -\varepsilon \cos^2[\pi(r - r_c)/2w_c], \quad r_c \le r \le r_c + w_c$$

with $w_c = 1.6\sigma$. Due to the soft attraction (strength $\varepsilon = 0.8k_BT$), side chains and lipids tended to display moderate aggregation, remaining in the liquid state rather than forming a solid.

When studying the landing process *via* steered molecular dynamics, we confined the lipid headgroups of the outer leaflet of the membrane within the $x-y$ plane, and simultaneously fixed the center of mass of the peptide core but released all other degrees of freedom. By systematically varying the distance between the peptide and the membrane, we could measure the free-energy change upon landing. Here the system was examined in the *NVT* ensemble by applying a Langevin thermostat to introduce thermal fluctuations. In the subsequent investigation of the insertion process, to allow the reconfiguration of the membrane upon insertion, we also applied a Berendsen barostat and kept the system under constant pressure, equal to the osmotic pressure of a 100 mM salt solution. All simulations were performed for more than 10^7 time steps, with time step $dt = 0.002\tau$, where $\tau = (m\sigma^2/\varepsilon)^{1/2}$ (m the bead mass) was the LJ time unit.

SAXS Experiments. SUVs were prepared from lyophilized phospholipids DOPS (1,2-dioleoyl-*sn*-glycero-3-phospho-L-serine (sodium salt)) and DOPE (1,2-dioleoyl-*sn*-glycero-3-phosphoethanolamine) purchased from Avanti Polar Lipids. Briefly, individual lipid stock solutions were prepared by dissolving DOPS and DOPE in chloroform at 20 mg/mL. A model membrane composition was prepared from the lipid stock solutions as a mixture of DOPS/DOPE at a 20/80 molar ratio. The lipid mixture was evaporated under N_2 and desiccated under vacuum overnight to form a lipid film, and then resuspended in aqueous 100 mM NaCl, 10 mM *N*-(2-hydroxyethyl)-piperazine-*N*′-ethanesulfonic acid (HEPES) (pH 7.4) to a concentration of 20 mg/mL. The aqueous lipid suspension was incubated at 37 °C overnight, sonicated until clear, and extruded through a 0.2 μm pore Nucleopore filter (Whatman) to obtain SUVs.

Metaphilic peptides were solubilized in aqueous 100 mM NaCl, 10 mM HEPES (pH 7.4) and mixed with SUVs at electroneutral P/L molar ratios, which are calculated based on 20 mol % of lipids having anionic charge. Samples were hermetically sealed into quartz capillaries (Hilgenberg GmbH, Mark-tubes) for SAXS experiments at the Stanford Synchrotron Radiation Lightsource (SSRL, beamline 4−2) using monochromatic X-rays with an energy of 9 keV. Scattered radiation was collected using a Rayonix MX255-HE detector (73.2 μm pixel size) and 2D SAXS powder patterns were integrated with Nika 1.50[100] package for Igor Pro 6.31 and FIT2D.[101]

The integrated scattering intensity $I(Q)$ was plotted against Q using Origin Lab software. Phases present in each sample were identified by tabulating the measured peak positions, Q_{measured}, and comparing their ratios with those of the permitted reflections for different crystal phases. The lattice parameter of each identified phase was calculated from the slope of the linear regression through points corresponding to the peaks. For powder-averaged cubic and hexagonal phases, each point corresponding to a peak was defined by coordinates of the assigned reflection (in terms of Miller indices h, k, l) and Q_{measured}. For a cubic phase, $Q = (2\pi/a)\sqrt{(h^2 + k^2 + l^2)}$, and for a hexagonal phase, $Q = (4\pi/(a\sqrt{3}))\sqrt{(h^2 + hk + k^2)}$, where a is the lattice parameter. Therefore, the slopes of the regressions of Q_{measured} *vs* $\sqrt{(h^2 + k^2 + l^2)}$ and Q_{measured} *vs* $\sqrt{(h^2 + hk + k^2)}$ are $2\pi/a$ and $4\pi/(a\sqrt{3})$, respectively, which can be used to calculate a. For a lamellar phase, each point corresponding to a peak has coordinates of the order of the reflection, N, and Q_{measured} with the relation $Q = 2\pi N/d$. The regression of Q_{measured} *vs* N then has a slope of $2\pi/d$, which yields the periodic spacing d.

Cellular Uptake Experiments. Cellular uptake data were sourced from experiments conducted previously elsewhere[45] to be compared with findings from this study. Briefly, HeLa cells were seeded into 96-well plates at a density of 1×10^4 cells/well and cultured for 24 h. The culture medium was then replaced with serum-free Dulbecco's modified Eagle's medium (DMEM). Endocytosis inhibitors chlorpromazine (10 μg/mL), genistein (200 μg/mL), methyl-β-cyclodextrin (50 μM), and wortmannin (50 nM) were added to the cells 30 min before the addition of peptide. To investigate the membrane permeability, each peptide was labeled with rhodamine (RhB) and 2 μg was added into each well containing HeLa cells. After incubating the RhB-peptide with the cells for 2 h at 37 °C, the cells were washed with phosphate-buffered saline (PBS) containing 20 U/mL heparin and then lysed using radioimmunoprecipitation assay (RIPA) buffer at room temperature for 20 min. The intracellular content of the RhB-peptide in the cell lysate was quantified using spectrofluorimetry and the cellular protein level was quantified using a bicinchoninic acid (BCA) kit, such that the uptake level was expressed as the quantity (μg) of RhB-peptide per 1 mg of cellular protein. Peptide-induced pore formation in cell membranes was studied by measuring the cellular internalization of membrane-impermeable FITC. The procedures were the same as above, except 2 μg of peptide and 0.2 μg of FITC were added into each well containing HeLa cells. Cells that were treated with only FITC served as the control. FITC in the cell lysate was quantified using spectrofluorimetry and the uptake level was expressed as the quantity (μg) of FITC per 1 mg of cellular protein. The cellular uptake levels were compared against those of HIV-TAT and R9 that had been fluorescently labeled with carboxytetramethylrhodamine (TAMRA).

Calculation of Hydrophobic Volume for Metaphilic Peptide Comparisons. We defined the hydrophobic volume of a metaphilic peptide by the total number of methyl and/or methylene groups present among its side chains. For uncharged side chains, this includes: (a) R, conjugated alkyl chain with 4−6 hydrocarbons, (b) $x + 2$, spacer between triazole and ester with 3, 6, or 8 methylene groups, (c) spacer between backbone and ester with 2 methylene groups. For charged side chains, this includes: (a) spacer between triazole and guanidine

DOI: 10.1021/acsnano.6b07981
ACS Nano 2017, 11, 2858−2871

with 1 methylene group, (b) $x + 2$, spacer between triazole and ester with 3, 6, or 8 methylene groups, (c) spacer between backbone and ester with 2 methylene groups. For example, for metaphilic peptide P11: (0.5)(69)(5 + 3 + 2) + (0.5)(69)(1 + 3 + 2) = 552 total methyl and/or methylene groups.

Mean-Field Theory. We employed a molecular lipid model that was proposed and analyzed in previous work.[94] It describes the free energy per lipid

$$f(a_i, a_h, b) = \gamma a_i + \frac{B}{a_h} + \tau(b - l_c)^2 \quad (1)$$

in a lipid bilayer as a function of three molecular quantities, a_i, a_h, and b; see Figure 5A. The first contribution to f corresponds to the interfacial energy of exposing the apolar hydrocarbon chains to the polar headgroup region; a_i is the cross-sectional area per lipid at this interface, and $\gamma \approx 12 k_B T/\text{nm}^2$ is the corresponding surface tension. The second term accounts for the repulsive interactions between lipid headgroups, described in terms of a single headgroup interaction surface of cross-sectional area a_h per lipid, located a fixed distance l_h away from the interface between the hydrocarbon chains and headgroups. All headgroup interactions (steric, ionic, dipolar, hydration, *etc.*) are lumped into a single parameter, B. Finally, the third term in eq 1 describes the stretching/compression energy of the hydrocarbon chain region, where b is the actual thickness and l_c the preferred thickness of the hydrocarbon core for each membrane leaflet. The prefactor τ and the preferred thickness l_c have been previously estimated using detailed molecular-level chain packing calculations,[94] resulting in $\tau = 7.9 k_B T/\text{nm}^2$ and $l_c = 1.16$ nm for lipids with two $-(CH_2)_{15}-CH_3$ hydrocarbon chains. We also assumed that the hydrophobic volume per lipid, $v_L = 0.918$ nm^3, is conserved for any given conformation a_i, a_h, and b. The bending free energy per unit area of an initially planar and symmetric lipid bilayer

$$\frac{\Delta f_E}{a_E} + \frac{\Delta f_I}{a_I} = \frac{\kappa}{2}(c_1 + c_2)^2 + \bar{\kappa} c_1 c_2 \quad (2)$$

can be expressed[102] in terms of the two principal curvatures c_1 and c_2, measured at the bilayer midplane, with κ and $\bar{\kappa}$ denoting the bending stiffness and Gaussian modulus, respectively. The left-hand side of eq 2 separates the free energy into contributions from the external (E) and internal (I) leaflet of the lipid bilayer. We characterized the lipid conformation in the external leaflet by a_i^E, a_h^E, b_E and in the internal leaflet by a_i^I, a_h^I, b_I. Knowing these quantities allowed us to calculate the bending-induced change in free energy per lipid, $\Delta f_E = f(a_i^E, a_h^E, b_E) - f(a_0, a_0, b_0)$ and $\Delta f_I = f(a_i^I, a_h^I, b_I) - f(a_0, a_0, b_0)$, in the external and internal leaflet, respectively, where a_0 is the equilibrium cross-sectional area per lipid of a planar membrane. Note that the conservation of the hydrophobic volume per lipid, v_L, links $a_0 = v_L/b_0$ to the equilibrium chain extension b_0 in a planar membrane. More generally, for nonvanishing membrane curvatures, conservation of v_L links the cross-sectional areas $a_E = v_L/\{b_E[1 + (c_1 + c_2)b_E/2 + c_1 c_2 b_E^2/3]\}$ and $a_I = v_L/\{b_I[1 - (c_1 + c_2)b_I/2 + c_1 c_2 b_I^2/3]\}$ of the lipids in the external and internal leaflets, measured at the bilayer midplane, to their respective chain lengths b_E and b_I. In fact, the molecular cross-sectional areas $a_i^E = a_E[1 + (c_1 + c_2)b_E + c_1 c_2 b_E^2]$, $a_i^I = a_I[1 - (c_1 + c_2)b_I + c_1 c_2 b_I^2]$, $a_h^E = a_E[1 + (c_1 + c_2)(b_E + l_h) + c_1 c_2 (b_E + l_h)^2]$, and $a_h^I = a_I[1 - (c_1 + c_2)(b_I + l_h) + c_1 c_2 (b_I + l_h)^2]$ can all be related to b_E and b_I through simple geometric relations. Yet, the hydrophobic thicknesses $b_E = b_0[1 + \eta(c_1 + c_2)]$ and $b_I = b_0[1 - \eta(c_1 + c_2)]$ of the external and internal leaflets, respectively, may themselves be curvature-dependent. We accounted for the curvature-induced adjustment of leaflet thickness through a yet unknown relaxation parameter η. The free energy in eq 2 adopts its minimum with respect to η. Force equilibrium of a planar membrane yields the condition

$$B = \frac{\gamma v_L^2}{b_0^2} - 2\tau v_L (b_0 - l_c) \quad (3)$$

for the equilibrium thickness b_0. Typical values for the equilibrium cross-sectional area per lipid of a planar membrane, $a_0 \approx 0.7$ nm^2, are well-known from both experiments[103] and MD simulations.[104] Hence, we used $b_0 = v_L/a_0 = 1.31$ nm as input in eq 3 to determine the headgroup repulsion parameter B.

Series expansion of the left-hand side of eq 2, minimization with respect to η, and comparison with the right-hand side of that equation allowed us to calculate the Gaussian modulus $\bar{\kappa}$, the relaxation parameter η, and the bending stiffness κ. It was convenient to express the results in terms of the dimensionless quantities $\bar{B} = B b_0^2/(\gamma v_L^2)$, $\bar{\tau} = \tau b_0^3/(\gamma v_L)$, $\bar{l}_c = l_c/b_0$, and $\bar{l}_h = l_h/b_0$. Eq 3 was then equivalent to $\bar{B} = 1 - 2\bar{\tau}(1 - \bar{l}_c)$. With that, our final results are

$$\bar{\kappa} = \frac{2}{3} b_0^2 \gamma \{2(1 - \bar{l}_c)[2 + 3\bar{l}_h(2 + \bar{l}_h)]\bar{\tau} - 3\bar{l}_h(2 + \bar{l}_h)\} \quad (4)$$

$$\eta = \frac{b_0}{2} \frac{1 + 2\bar{l}_h - (1 - \bar{l}_c)(3 + 4\bar{l}_h)\bar{\tau}}{1 + \bar{\tau}}$$

$$\kappa = \gamma b_0^2 \left\{ (1 + 2\bar{l}_h)^2 [1 + 2(\bar{l}_c - 1)\bar{\tau}] - \frac{[1 + 2\bar{l}_h + (\bar{l}_c - 1)(3 + 4\bar{l}_h)\bar{\tau}]^2}{1 + \bar{\tau}} \right\}$$

As introduced above, we used $\gamma = 12 k_B T/\text{nm}^2$, $\tau = 7.9 k_B T/\text{nm}^2$, $l_c = 1.16$ nm, $v_L = 0.918$ nm^3, and $b_0 = 1.31$ nm. With that, we obtained the following values for $\bar{\kappa}$, η, and κ as functions of the distance l_h between the headgroup interaction surface and the polar−apolar interface (Table 1).

Table 1. Values for $\bar{\kappa}$, η, and κ as Functions of l_h

l_h (nm)	$\bar{\kappa}$ ($k_B T$)	η (b_0)	κ ($k_B T$)
0.1	6.0	0.14	14.9
0.3	−3.1	0.18	23.3
0.5	−13.5	0.23	33.6

A small headgroup, such as for $l_h = 0.1$ nm, entails a positive Gaussian modulus and thus instability with respect to NGC. Growing headgroup size increases the bending stiffness and decreases the Gaussian modulus to more negative values. In the following we use $l_h = 0.3$ nm.

Metaphilic peptides insert into the hydrocarbon core of the host bilayer such that their hydrophobic moieties are buried into the hydrocarbon core whereas the charged groups extend toward the polar−apolar interface. The burying of the peptide into the hydrocarbon core is described in our model by an effective increase in the lipid's hydrophobic volume $v_L \to v_L + v_P^{\text{eff}} P/L$, where P/L is the peptide-to-lipid ratio and v_P^{eff} is the effective hydrophobic volume of the peptide. If the peptide's monomers were all hydrophobic, $v_P^{\text{eff}} = v_P$ would correspond to the hydrophobic volume of the peptide, $v_P = 15$ nm^3 for P11. The effective value v_P^{eff} is expected to be somewhat smaller than v_P, depending on how much area the charged groups occupy at the membrane's polar−apolar interface and at the headgroup interaction surface. The electrostatic interactions of the cationic side chains with the anionic lipid headgroups can be described within the classical Poisson−Boltzmann theory. As noted by Israelachvili,[93] the inverse $1/a_h$-dependence of the headgroup repulsion free-energy contribution is consistent with the linearized Poisson−Boltzmann model, which is applicable for membranes with mole fractions of up to 20% of charged lipids at physiological conditions.[105] This simply implies replacement of the headgroup repulsion parameter in eq 1 by $B - k_B T 2\pi l_B l_D [\phi^2 - (\phi - z_c P/L)^2]$, where $l_B = 0.7$ nm is the Bjerrum length in water, $l_D = 1$ nm is the Debye screening length at physiological conditions, and $z_c = +35$ is the number of cationic side chains in P11. We also recall that $\phi = 0.2$ is the mole fraction of anionic lipids. Figure 5B was then calculated for $v_P^{\text{eff}} = 10$ nm^3 and $z_c = +35$ (solid line), $v_P^{\text{eff}} = 10$ nm^3 and $z_c = 0$ (dashed line), and $v_P^{\text{eff}} = 0$ and $z_c = +35$ (dash-dotted line). A more systematic description of the Gaussian modulus and the bending stiffness for

DOI: 10.1021/acsnano.6b07981
ACS Nano 2017, 11, 2858−2871

variations of v_P^{eff} and z_c is presented in Figure S1 of the Supporting Information, and suggests that insertion of metaphilic peptides into membranes generally tends to shift the Gaussian modulus toward less negative values but has little effect on the bending stiffness.

ASSOCIATED CONTENT

Supporting Information

The Supporting Information is available free of charge on the ACS Publications website at DOI: 10.1021/acsnano.6b07981.

Scheme S1; Figure S1 (PDF)

AUTHOR INFORMATION

Corresponding Author

*E-mail: gclwong@seas.ucla.edu.

ORCID

Michelle W. Lee: 0000-0003-1613-9501

Lichen Yin: 0000-0002-4573-0555

Present Addresses

□Key Laboratory of Polymeric Materials and Application Technology of Hunan Province, Key Laboratory of Advanced Functional Polymer Materials of Colleges and Universities of Hunan Province, College of Chemistry, Xiangtan University, Xiangtan, Hunan 411105, China.

▲Institute of Functional Nano and Soft Materials, Soochow University, Suzhou, Jiangsu 215123, China.

Notes

The authors declare no competing financial interest.

ACKNOWLEDGMENTS

This work is supported by grants from the National Science Foundation (DMR-1411329 to M.W.L. and G.C.L.W.; DMR-1610796 to M.H. and E.L.; DMR-1309525 to J.C.) and the National Institutes of Health (1R21AI117080 to J.C.). G.V.B. acknowledges a doctoral scholarship from CAPES Foundation/Brazil Ministry of Education (Grant No. 9466/13-4). Use of the Stanford Synchrotron Radiation Lightsource, SLAC National Accelerator Laboratory, is supported by the U.S. Department of Energy, Office of Science, Office of Basic Energy Sciences under Contract No. DE-AC02-76SF00515. The SSRL Structural Molecular Biology Program is supported by the DOE Office of Biological and Environmental Research, and by the National Institutes of Health, National Institute of General Medical Sciences (including P41GM103393).

REFERENCES

(1) Zeiger, A. S.; Layton, B. E. Molecular Modeling of the Axial and Circumferential Elastic Moduli of Tubulin. *Biophys. J.* **2008**, *95*, 3606−3618.

(2) Guthold, M.; Liu, W.; Sparks, E. A.; Jawerth, L. M.; Peng, L.; Falvo, M.; Superfine, R.; Hantgan, R. R.; Lord, S. T. A Comparison of the Mechanical and Structural Properties of Fibrin Fibers with Other Protein Fibers. *Cell Biochem. Biophys.* **2007**, *49*, 165−181.

(3) Gittes, F.; Mickey, B.; Nettleton, J.; Howard, J. Flexural Rigidity of Microtubules and Actin Filaments Measured from Thermal Fluctuations in Shape. *J. Cell Biol.* **1993**, *120*, 923−934.

(4) Vitkup, D.; Ringe, D.; Petsko, G. A.; Karplus, M. Solvent Mobility and the Protein 'Glass' Transition. *Nat. Struct. Biol.* **2000**, *7*, 34−38.

(5) Ringe, D.; Petsko, G. A. The 'Glass Transition' in Protein Dynamics: What It Is, Why It Occurs, and How to Exploit It. *Biophys. Chem.* **2003**, *105*, 667−680.

(6) Zasloff, M. Antimicrobial Peptides of Multicellular Organisms. *Nature* **2002**, *415*, 389−395.

(7) Brogden, K. A. Antimicrobial Peptides: Pore Formers or Metabolic Inhibitors in Bacteria? *Nat. Rev. Microbiol.* **2005**, *3*, 238−250.

(8) Hancock, R. E. W.; Sahl, H.-G. Antimicrobial and Host-Defense Peptides As New Anti-Infective Therapeutic Strategies. *Nat. Biotechnol.* **2006**, *24*, 1551−1557.

(9) Yeaman, M. R.; Yount, N. Y. Mechanisms of Antimicrobial Peptide Action and Resistance. *Pharmacol. Rev.* **2003**, *55*, 27−55.

(10) Lee, M. W.; Schmidt, N. W. Mechanisms of Membrane Curvature Generation by Peptides and Proteins: A Unified Perspective on Antimicrobial Peptides. In *Handbook of Lipid Membranes: Molecular, Functional, and Materials Aspects*; Safinya, C. R., Radler, J., Eds.; Taylor and Francis, in press.

(11) Shai, Y. Mechanism of the Binding, Insertion and Destabilization of Phospholipid Bilayer Membranes by α-Helical Antimicrobial and Cell Non-Selective Membrane-Lytic Peptides. *Biochim. Biophys. Acta, Biomembr.* **1999**, *1462*, 55−70.

(12) Hancock, R. E. W.; Lehrer, R. Cationic Peptides: A New Source of Antibiotics. *Trends Biotechnol.* **1998**, *16*, 82−88.

(13) Milletti, F. Cell-Penetrating Peptides: Classes, Origin, and Current Landscape. *Drug Discovery Today* **2012**, *17*, 850−860.

(14) Koren, E.; Torchilin, V. P. Cell-Penetrating Peptides: Breaking through to the Other Side. *Trends Mol. Med.* **2012**, *18*, 385−393.

(15) Bechara, C.; Sagan, S. Cell-Penetrating Peptides: 20 Years Later, Where Do We Stand? *FEBS Lett.* **2013**, *587*, 1693−1702.

(16) Futaki, S.; Suzuki, T.; Ohashi, W.; Yagami, T.; Tanaka, S.; Ueda, K.; Sugiura, Y. Arginine-Rich Peptides: An Abundant Source of Membrane-Permeable Peptides Having Potential As Carriers for Intracellular Protein Delivery. *J. Biol. Chem.* **2001**, *276*, 5836−5840.

(17) Wender, P. A.; Galliher, W. C.; Goun, E. A.; Jones, L. R.; Pillow, T. H. The Design of Guanidinium-Rich Transporters and Their Internalization Mechanisms. *Adv. Drug Delivery Rev.* **2008**, *60*, 452−472.

(18) Copolovici, D. M.; Langel, K.; Eriste, E.; Langel, Ü. Cell-Penetrating Peptides: Design, Synthesis, and Applications. *ACS Nano* **2014**, *8*, 1972−1994.

(19) Pooga, M.; Langel, Ü. Classes of Cell-Penetrating Peptides. In *Cell-Penetrating Peptides: Methods and Protocols*; Langel, Ü., Ed.; Springer New York: New York, NY, 2015; pp 3−28.

(20) Lee, E. Y.; Fulan, B. M.; Wong, G. C. L.; Ferguson, A. L. Mapping Membrane Activity in Undiscovered Peptide Sequence Space Using Machine Learning. *Proc. Natl. Acad. Sci. U. S. A.* **2016**, *113*, 13588−13593.

(21) Schmidt, N. W.; Mishra, A.; Wang, J.; DeGrado, W. F.; Wong, G. C. L. Influenza Virus A M2 Protein Generates Negative Gaussian Membrane Curvature Necessary for Budding and Scission. *J. Am. Chem. Soc.* **2013**, *135*, 13710−13719.

(22) Yao, H.; Lee, M. W.; Waring, A. J.; Wong, G. C. L.; Hong, M. Viral Fusion Protein Transmembrane Domain Adopts β-Strand Structure to Facilitate Membrane Topological Changes for Virus−Cell Fusion. *Proc. Natl. Acad. Sci. U. S. A.* **2015**, *112*, 10926−10931.

(23) Xiong, M.; Lee, M. W.; Mansbach, R. A.; Song, Z.; Bao, Y.; Peek, R. M.; Yao, C.; Chen, L.-F.; Ferguson, A. L.; Wong, G. C. L.; Cheng, J. Helical Antimicrobial Polypeptides with Radial Amphiphilicity. *Proc. Natl. Acad. Sci. U. S. A.* **2015**, *112*, 13155−13160.

(24) Lam, S. J.; O'Brien-Simpson, N. M.; Pantarat, N.; Sulistio, A.; Wong, E. H. H.; Chen, Y.-Y.; Lenzo, J. C.; Holden, J. A.; Blencowe, A.; Reynolds, E. C.; Qiao, G. G. Combating Multidrug-Resistant Gram-Negative Bacteria with Structurally Nanoengineered Antimicrobial Peptide Polymers. *Nat. Microbiol.* **2016**, *1*, 16162.

(25) Zhao, K.; Choe, U.-J.; Kamei, D. T.; Wong, G. C. L. Enhanced Activity of Cyclic Transporter Sequences Driven by Phase Behavior of Peptide-Lipid Complexes. *Soft Matter* **2012**, *8*, 6430−6433.

(26) Saleh, A. F.; Arzumanov, A.; Abes, R.; Owen, D.; Lebleu, B.; Gait, M. J. Synthesis and Splice-Redirecting Activity of Branched, Arginine-Rich Peptide Dendrimer Conjugates of Peptide Nucleic Acid Oligonucleotides. *Bioconjugate Chem.* **2010**, *21*, 1902−1911.

DOI: 10.1021/acsnano.6b07981
ACS Nano 2017, 11, 2858−2871

(27) Mandal, D.; Nasrolahi Shirazi, A.; Parang, K. Cell-Penetrating Homochiral Cyclic Peptides As Nuclear-Targeting Molecular Transporters. *Angew. Chem., Int. Ed.* **2011**, *50*, 9633−9637.
(28) Angeles-Boza, A. M.; Erazo-Oliveras, A.; Lee, Y.-J.; Pellois, J.-P. Generation of Endosomolytic Reagents by Branching of Cell-Penetrating Peptides: Tools for the Delivery of Bioactive Compounds to Live Cells in Cis or Trans. *Bioconjugate Chem.* **2010**, *21*, 2164−2167.
(29) Lindemann, F. A. The Calculation of Molecular Vibration Frequencies. *Phys. Z.* **1910**, *11*, 609−612.
(30) Bilgram, J. H. Dynamics at the Solid-Liquid Transition: Experiments at the Freezing Point. *Phys. Rep.* **1987**, *153*, 1−89.
(31) Zhou, Y.; Karplus, M. Folding Thermodynamics of a Model Three-Helix-Bundle Protein. *Proc. Natl. Acad. Sci. U. S. A.* **1997**, *94*, 14429−14432.
(32) We note that the "quasi-liquid" layer is not necessarily a liquid defined in terms of translational and orientational degrees of freedom. The term is borrowed from the phenomenon of surface melting,[33,34] which uses the Lindemann criterion to define a "molten" quasi-liquid layer.
(33) Lipowsky, R. Critical Surface Phenomena at First-Order Bulk Transitions. *Phys. Rev. Lett.* **1982**, *49*, 1575−1578.
(34) Frenken, J. W. M.; van der Veen, J. F. Observation of Surface Melting. *Phys. Rev. Lett.* **1985**, *54*, 134−137.
(35) Leslie, D. C.; Waterhouse, A.; Berthet, J. B.; Valentin, T. M.; Watters, A. L.; Jain, A.; Kim, P.; Hatton, B. D.; Nedder, A.; Donovan, K.; Super, E. H.; Howell, C.; Johnson, C. P.; Vu, T. L.; Bolgen, D. E.; Rifai, S.; Hansen, A. R.; Aizenberg, M.; Super, M.; Aizenberg, J.; et al. A Bioinspired Omniphobic Surface Coating on Medical Devices Prevents Thrombosis and Biofouling. *Nat. Biotechnol.* **2014**, *32*, 1134−1140.
(36) MacCallum, N.; Howell, C.; Kim, P.; Sun, D.; Friedlander, R.; Ranisau, J.; Ahanotu, O.; Lin, J. J.; Vena, A.; Hatton, B.; Wong, T.-S.; Aizenberg, J. Liquid-Infused Silicone As a Biofouling-Free Medical Material. *ACS Biomater. Sci. Eng.* **2015**, *1*, 43−51.
(37) Nosonovsky, M. Materials Science: Slippery When Wetted. *Nature* **2011**, *477*, 412−413.
(38) Munoz, V.; Blanco, F. J.; Serrano, L. The Hydrophobic-Staple Motif and a Role for Loop-Residues in α-Helix Stability and Protein Folding. *Nat. Struct. Biol.* **1995**, *2*, 380−385.
(39) Matsuzaki, K.; Nakamura, A.; Murase, O.; Sugishita, K.; Fujii, N.; Miyajima, K. Modulation of Magainin 2−Lipid Bilayer Interactions by Peptide Charge. *Biochemistry* **1997**, *36*, 2104−2111.
(40) Chiti, F.; Stefani, M.; Taddei, N.; Ramponi, G.; Dobson, C. M. Rationalization of the Effects of Mutations on Peptide and Protein Aggregation Rates. *Nature* **2003**, *424*, 805−808.
(41) Chen, Y.; Mant, C. T.; Farmer, S. W.; Hancock, R. E. W.; Vasil, M. L.; Hodges, R. S. Rational Design of α-Helical Antimicrobial Peptides with Enhanced Activities and Specificity/Therapeutic Index. *J. Biol. Chem.* **2005**, *280*, 12316−12329.
(42) Yin, L. M.; Edwards, M. A.; Li, J.; Yip, C. M.; Deber, C. M. Roles of Hydrophobicity and Charge Distribution of Cationic Antimicrobial Peptides in Peptide-Membrane Interactions. *J. Biol. Chem.* **2012**, *287*, 7738−7745.
(43) Lu, H.; Wang, J.; Bai, Y.; Lang, J. W.; Liu, S.; Lin, Y.; Cheng, J. Ionic Polypeptides with Unusual Helical Stability. *Nat. Commun.* **2011**, *2*, 206.
(44) Gabrielson, N. P.; Lu, H.; Yin, L.; Li, D.; Wang, F.; Cheng, J. Reactive and Bioactive Cationic α-Helical Polypeptide Template for Nonviral Gene Delivery. *Angew. Chem., Int. Ed.* **2012**, *51*, 1143−1147.
(45) Tang, H.; Yin, L.; Kim, K. H.; Cheng, J. Helical Poly(Arginine) Mimics with Superior Cell-Penetrating and Molecular Transporting Properties. *Chem. Sci.* **2013**, *4*, 3839−3844.
(46) Bechinger, B. Rationalizing the Membrane Interactions of Cationic Amphipathic Antimicrobial Peptides by Their Molecular Shape. *Curr. Opin. Colloid Interface Sci.* **2009**, *14*, 349−355.
(47) Dathe, M.; Schümann, M.; Wieprecht, T.; Winkler, A.; Beyermann, M.; Krause, E.; Matsuzaki, K.; Murase, O.; Bienert, M. Peptide Helicity and Membrane Surface Charge Modulate the Balance of Electrostatic and Hydrophobic Interactions with Lipid Bilayers and Biological Membranes. *Biochemistry* **1996**, *35*, 12612−12622.
(48) Segrest, J. P.; De Loof, H.; Dohlman, J. G.; Brouillette, C. G.; Anantharamaiah, G. M. Amphipathic Helix Motif: Classes and Properties. *Proteins: Struct., Funct., Genet.* **1990**, *8*, 103−117.
(49) Tytler, E. M.; Segrest, J. P.; Epand, R. M.; Nie, S. Q.; Epand, R. F.; Mishra, V. K.; Venkatachalapathi, Y. V.; Anantharamaiah, G. M. Reciprocal Effects of Apolipoprotein and Lytic Peptide Analogs on Membranes. Cross-Sectional Molecular Shapes of Amphipathic α Helixes Control Membrane Stability. *J. Biol. Chem.* **1993**, *268*, 22112−22118.
(50) Zimmerberg, J.; Kozlov, M. M. How Proteins Produce Cellular Membrane Curvature. *Nat. Rev. Mol. Cell Biol.* **2006**, *7*, 9−19.
(51) Campelo, F.; McMahon, H. T.; Kozlov, M. M. The Hydrophobic Insertion Mechanism of Membrane Curvature Generation by Proteins. *Biophys. J.* **2008**, *95*, 2325−2339.
(52) Zemel, A.; Ben-Shaul, A.; May, S. Modulation of the Spontaneous Curvature and Bending Rigidity of Lipid Membranes by Interfacially Adsorbed Amphipathic Peptides. *J. Phys. Chem. B* **2008**, *112*, 6988−6996.
(53) Epand, R. M.; Shai, Y.; Segrest, J. P.; Anantharamiah, G. M. Mechanisms for the Modulation of Membrane Bilayer Properties by Amphipathic Helical Peptides. *Biopolymers* **1995**, *37*, 319−338.
(54) Many AMPs are often disordered in aqueous solution. However, upon binding with membranes they adopt amphiphilic α-helical secondary structures with the helix axis parallel to the membrane surface. In this conformation, the hydrophobic and charged residues are segregated to opposite faces of the helix, which allows their interactions with the membrane core and lipid headgroups, respectively.[8,55,56]
(55) Bechinger, B. The Structure, Dynamics and Orientation of Antimicrobial Peptides in Membranes by Multidimensional Solid-State NMR Spectroscopy. *Biochim. Biophys. Acta, Biomembr.* **1999**, *1462*, 157−183.
(56) Gennaro, R.; Zanetti, M. Structural Features and Biological Activities of the Cathelicidin-Derived Antimicrobial Peptides. *Biopolymers* **2000**, *55*, 31−49.
(57) Chen, H.-C.; Brown, J. H.; Morell, J. L.; Huang, C. M. Synthetic Magainin Analogues with Improved Antimicrobial Activity. *FEBS Lett.* **1988**, *236*, 462−466.
(58) Blondelle, S. E.; Houghten, R. A. Design of Model Amphipathic Peptides Having Potent Antimicrobial Activities. *Biochemistry* **1992**, *31*, 12688−12694.
(59) Drin, G.; Antonny, B. Amphipathic Helices and Membrane Curvature. *FEBS Lett.* **2010**, *584*, 1840−1847.
(60) Schmidt, N. W.; Wong, G. C. L. Antimicrobial Peptides and Induced Membrane Curvature: Geometry, Coordination Chemistry, and Molecular Engineering. *Curr. Opin. Solid State Mater. Sci.* **2013**, *17*, 151−163.
(61) Schmidt, N. W.; Lis, M.; Zhao, K.; Lai, G. H.; Alexandrova, A. N.; Tew, G. N.; Wong, G. C. L. Molecular Basis for Nanoscopic Membrane Curvature Generation from Quantum Mechanical Models and Synthetic Transporter Sequences. *J. Am. Chem. Soc.* **2012**, *134*, 19207−19216.
(62) Mishra, A.; Lai, G. H.; Schmidt, N. W.; Sun, V. Z.; Rodriguez, A. R.; Tong, R.; Tang, L.; Cheng, J.; Deming, T. J.; Kamei, D. T.; Wong, G. C. L. Translocation of HIV TAT Peptide and Analogues Induced by Multiplexed Membrane and Cytoskeletal Interactions. *Proc. Natl. Acad. Sci. U. S. A.* **2011**, *108*, 16883−16888.
(63) Schmidt, N. W.; Mishra, A.; Lai, G. H.; Davis, M.; Sanders, L. K.; Tran, D.; Garcia, A.; Tai, K. P.; McCray, P. B.; Ouellette, A. J.; Selsted, M. E.; Wong, G. C. L. Criterion for Amino Acid Composition of Defensins and Antimicrobial Peptides Based on Geometry of Membrane Destabilization. *J. Am. Chem. Soc.* **2011**, *133*, 6720−6727.
(64) Schmidt, N.; Mishra, A.; Lai, G. H.; Wong, G. C. L. Arginine-Rich Cell-Penetrating Peptides. *FEBS Lett.* **2010**, *584*, 1806−1813.
(65) Schmidt, N. W.; Tai, K. P.; Kamdar, K.; Mishra, A.; Lai, G. H.; Zhao, K.; Ouellette, A. J.; Wong, G. C. L. Arginine in α-Defensins: Differential Effects on Bactericidal Activity Correspond to Geometry

DOI: 10.1021/acsnano.6b07981
ACS Nano 2017, 11, 2858−2871

of Membrane Curvature Generation and Peptide-Lipid Phase Behavior. *J. Biol. Chem.* **2012**, *287*, 21866−21872.
(66) Mishra, A.; Gordon, V. D.; Yang, L.; Coridan, R.; Wong, G. C. L. HIV TAT Forms Pores in Membranes by Inducing Saddle-Splay Curvature: Potential Role of Bidentate Hydrogen Bonding. *Angew. Chem., Int. Ed.* **2008**, *47*, 2986−2989.
(67) Shearman, G. C.; Ces, O.; Templer, R. H.; Seddon, J. M. Inverse Lyotropic Phases of Lipids and Membrane Curvature. *J. Phys.: Condens. Matter* **2006**, *18*, S1105.
(68) *Micelles, Membranes, Microemulsions, and Monolayers*; Gelbart, W. M., Ben-Shaul, A., Roux, D., Eds.; Springer-Verlag: New York, 1994.
(69) Jenssen, H.; Hamill, P.; Hancock, R. E. W. Peptide Antimicrobial Agents. *Clin. Microbiol. Rev.* **2006**, *19*, 491−511.
(70) Hu, K.; Schmidt, N. W.; Zhu, R.; Jiang, Y.; Lai, G. H.; Wei, G.; Palermo, E. F.; Kuroda, K.; Wong, G. C. L.; Yang, L. A Critical Evaluation of Random Copolymer Mimesis of Homogeneous Antimicrobial Peptides. *Macromolecules* **2013**, *46*, 1908−1915.
(71) Lee, M. W.; Chakraborty, S.; Schmidt, N. W.; Murgai, R.; Gellman, S. H.; Wong, G. C. L. Two Interdependent Mechanisms of Antimicrobial Activity Allow for Efficient Killing in Nylon-3-Based Polymeric Mimics of Innate Immunity Peptides. *Biochim. Biophys. Acta, Biomembr.* **2014**, *1838*, 2269−2279.
(72) Yang, L.; Gordon, V. D.; Trinkle, D. R.; Schmidt, N. W.; Davis, M. A.; DeVries, C.; Som, A.; Cronan, J. E.; Tew, G. N.; Wong, G. C. L. Mechanism of a Prototypical Synthetic Membrane-Active Antimicrobial: Efficient Hole-Punching *via* Interaction with Negative Intrinsic Curvature Lipids. *Proc. Natl. Acad. Sci. U. S. A.* **2008**, *105*, 20595−20600.
(73) Tamba, Y.; Ariyama, H.; Levadny, V.; Yamazaki, M. Kinetic Pathway of Antimicrobial Peptide Magainin 2-Induced Pore Formation in Lipid Membranes. *J. Phys. Chem. B* **2010**, *114*, 12018−12026.
(74) Hong, S.; Leroueil, P. R.; Janus, E. K.; Peters, J. L.; Kober, M.-M.; Islam, M. T.; Orr, B. G.; Baker, J. R.; Banaszak Holl, M. M. Interaction of Polycationic Polymers with Supported Lipid Bilayers and Cells: Nanoscale Hole Formation and Enhanced Membrane Permeability. *Bioconjugate Chem.* **2006**, *17*, 728−734.
(75) Takechi, Y.; Yoshii, H.; Tanaka, M.; Kawakami, T.; Aimoto, S.; Saito, H. Physicochemical Mechanism for the Enhanced Ability of Lipid Membrane Penetration of Polyarginine. *Langmuir* **2011**, *27*, 7099−7107.
(76) Herce, H. D.; Garcia, A. E. Molecular Dynamics Simulations Suggest a Mechanism for Translocation of the HIV-1 TAT Peptide Across Lipid Membranes. *Proc. Natl. Acad. Sci. U. S. A.* **2007**, *104*, 20805−20810.
(77) Herce, H. D.; Garcia, A. E. Cell Penetrating Peptides: How Do They Do It? *J. Biol. Phys.* **2007**, *33*, 345.
(78) Herce, H. D.; Garcia, A. E.; Litt, J.; Kane, R. S.; Martin, P.; Enrique, N.; Rebolledo, A.; Milesi, V. Arginine-Rich Peptides Destabilize the Plasma Membrane, Consistent with a Pore Formation Translocation Mechanism of Cell-Penetrating Peptides. *Biophys. J.* **2009**, *97*, 1917−1925.
(79) Matsuzaki, K.; Murase, O.; Miyajima, K. Kinetics of Pore Formation by an Antimicrobial Peptide, Magainin 2, in Phospholipid Bilayers. *Biochemistry* **1995**, *34*, 12553−12559.
(80) Tang, M.; Waring, A. J.; Hong, M. Phosphate-Mediated Arginine Insertion into Lipid Membranes and Pore Formation by a Cationic Membrane Peptide from Solid-State NMR. *J. Am. Chem. Soc.* **2007**, *129*, 11438−11446.
(81) Matsuzaki, K.; Murase, O.; Fujii, N.; Miyajima, K. Translocation of a Channel-Forming Antimicrobial Peptide, Magainin 2, across Lipid Bilayers by Forming a Pore. *Biochemistry* **1995**, *34*, 6521−6526.
(82) Deshayes, S.; Heitz, A.; Morris, M. C.; Charnet, P.; Divita, G.; Heitz, F. Insight into the Mechanism of Internalization of the Cell-Penetrating Carrier Peptide Pep-1 through Conformational Analysis. *Biochemistry* **2004**, *43*, 1449−1457.
(83) Bárány-Wallje, E.; Gaur, J.; Lundberg, P.; Langel, Ü.; Gräslund, A. Differential Membrane Perturbation Caused by the Cell Penetrating Peptide Tp10 Depending on Attached Cargo. *FEBS Lett.* **2007**, *581*, 2389−2393.
(84) Walrant, A.; Vogel, A.; Correia, I.; Lequin, O.; Olausson, B. E. S.; Desbat, B.; Sagan, S.; Alves, I. D. Membrane Interactions of Two Arginine-Rich Peptides with Different Cell Internalization Capacities. *Biochim. Biophys. Acta, Biomembr.* **2012**, *1818*, 1755−1763.
(85) Balayssac, S.; Burlina, F.; Convert, O.; Bolbach, G.; Chassaing, G.; Lequin, O. Comparison of Penetratin and Other Homeodomain-Derived Cell-Penetrating Peptides: Interaction in a Membrane-Mimicking Environment and Cellular Uptake Efficiency. *Biochemistry* **2006**, *45*, 1408−1420.
(86) Tiriveedhi, V.; Butko, P. A Fluorescence Spectroscopy Study on the Interactions of the TAT-PTD Peptide with Model Lipid Membranes. *Biochemistry* **2007**, *46*, 3888−3895.
(87) Mai, J. C.; Shen, H.; Watkins, S. C.; Cheng, T.; Robbins, P. D. Efficiency of Protein Transduction Is Cell Type-Dependent and Is Enhanced by Dextran Sulfate. *J. Biol. Chem.* **2002**, *277*, 30208−30218.
(88) Blondelle, S. E.; Lohner, K.; Aguilar, M.-I. Lipid-Induced Conformation and Lipid-Binding Properties of Cytolytic and Antimicrobial Peptides: Determination and Biological Specificity. *Biochim. Biophys. Acta, Biomembr.* **1999**, *1462*, 89−108.
(89) Wender, P. A.; Mitchell, D. J.; Pattabiraman, K.; Pelkey, E. T.; Steinman, L.; Rothbard, J. B. The Design, Synthesis, and Evaluation of Molecules That Enable or Enhance Cellular Uptake: Peptoid Molecular Transporters. *Proc. Natl. Acad. Sci. U. S. A.* **2000**, *97*, 13003−13008.
(90) Tünnemann, G.; Ter-Avetisyan, G.; Martin, R. M.; Stöckl, M.; Herrmann, A.; Cardoso, M. C. Live-Cell Analysis of Cell Penetration Ability and Toxicity of Oligo-Arginines. *J. Pept. Sci.* **2008**, *14*, 469−476.
(91) Mitchell, D. J.; Steinman, L.; Kim, D. T.; Fathman, C. G.; Rothbard, J. B. Polyarginine Enters Cells More efficiently than Other Polycationic Homopolymers. *J. Pept. Res.* **2000**, *56*, 318−325.
(92) Israelachvili, J. N.; Mitchell, D. J.; Ninham, B. W. Theory of Self-Assembly of Lipid Bilayers and Vesicles. *Biochim. Biophys. Acta, Biomembr.* **1977**, *470*, 185−201.
(93) Israelachvili, J. N. *Intermolecular and Surface Forces*, 2nd ed.; Academic Press, 1992.
(94) May, S. A Molecular Model for the Line Tension of Lipid Membranes. *Eur. Phys. J. E: Soft Matter Biol. Phys.* **2000**, *3*, 37−44.
(95) May, S.; Ben-Shaul, A. A Molecular Model for Lipid-Mediated Interaction between Proteins in Membranes. *Phys. Chem. Chem. Phys.* **2000**, *2*, 4494−4502.
(96) Lu, H.; Cheng, J. Hexamethyldisilazane-Mediated Controlled Polymerization of α-Amino Acid N-Carboxyanhydrides. *J. Am. Chem. Soc.* **2007**, *129*, 14114−14115.
(97) Lu, H.; Cheng, J. N-Trimethylsilyl Amines for Controlled Ring-Opening Polymerization of Amino Acid N-Carboxyanhydrides and Facile End Group Functionalization of Polypeptides. *J. Am. Chem. Soc.* **2008**, *130*, 12562−12563.
(98) Zasloff, M.; Adams, A. P.; Beckerman, B.; Campbell, A.; Han, Z.; Luijten, E.; Meza, I.; Julander, J.; Mishra, A.; Qu, W.; Taylor, J. M.; Weaver, S. C.; Wong, G. C. L. Squalamine As a Broad-Spectrum Systemic Antiviral Agent with Therapeutic Potential. *Proc. Natl. Acad. Sci. U. S. A.* **2011**, *108*, 15978−15983.
(99) Cooke, I. R.; Deserno, M. Solvent-Free Model for Self-Assembling Fluid Bilayer Membranes: Stabilization of the Fluid Phase Based on Broad Attractive Tail Potentials. *J. Chem. Phys.* **2005**, *123*, 224710.
(100) Ilavsky, J. Nika: Software for Two-Dimensional Data Reduction. *J. Appl. Crystallogr.* **2012**, *45*, 324−328.
(101) Hammersley, A. P. The FIT2D Home Page. http://www.esrf.eu/computing/scientific/FIT2D/. Accessed November 21, 2016.
(102) Helfrich, W. Elastic Properties of Lipid Bilayers: Theory and Possible Experiments. *Z. Naturforsch., C: J. Biosci.* **1973**, *28*, 693.
(103) Seddon, J. M.; Templer, R. H. Polymorphism of Lipid-Water Systems. In *Structure and Dynamics of Membranes*, 2nd ed.; Lipowsky, R., Sackmann, E., Eds.; Elsevier: Amsterdam, 1995; pp 98−160.
(104) Tieleman, D. P.; Marrink, S. J.; Berendsen, H. J. C. A Computer Perspective of Membranes: Molecular Dynamics Studies of

DOI: 10.1021/acsnano.6b07981
ACS Nano 2017, 11, 2858−2871

Lipid Bilayer Systems. *Biochim. Biophys. Acta, Rev. Biomembr.* **1997**, *1331*, 235−270.
(105) May, S. Lipid Membranes: Mean-Field Continuum Electrostatics. In *Encyclopedia of Surface and Colloid Science*, 3rd ed.; CRC Press, 2015; pp 3792−3806.

DOI: 10.1021/acsnano.6b07981
ACS Nano 2017, 11, 2858−2871